HYCELTEC 2022
VIII Symposium on Hydrogen, Fuel Cells and Advanced Batteries
Buenos Aires, July 11-14, 2022

8th Symposium on Hydrogen, Fuel Cells and Advanced Batteries, Buenos Aires, July 11th-14th, 2022

ZnO nanowires as photocatalyst for H_2 production from ethanol$_{(aq)}$ in gas phase (O-15H-V)

N. Homs[1,4*], A. C. Sola[1], P. R. Martínez-Alanis[1], X. Alcobé[2], F. Güell[3], P. Ramírez de la Piscina[1**]

[1] *Departament de Química Inorgànica i Orgànica, secció de Química Inorgànica and Institute of Nanoscience and Nanotechnology (IN2UB), Universitat de Barcelona, C/Martí i Franquès 1-11, 08028 Barcelona, Spain*

[2] *Scientific and Technological Centers (CCiTUB), C/Lluís Solé i Sabarís, 1-3, 08028 Barcelona, Spain*

[3] *Departament d'Enginyeria Electrònica i Biomèdica and Institute of Nanoscience and Nanotechnology (IN2UB), Universitat de Barcelona, C/Martí i Franquès 1-11, 08028 Barcelona, Spain*

[4] *Catalonia Institute for Energy Research (IREC), C/ Jardins de les Dones de Negre 1, 08930 Barcelona, Spain*

(*) Pres. author: narcis.homs@qi.ub.edu (**) Corresp. author: pilar.piscina@qi.ub.edu

Keywords: ZnO nanowires; photocatalytic H_2; H_2 from ethanol$_{(aq)}$; *in-situ* DRIFTS

1. Introduction

ZnO could be considered an interesting material for the photocatalytic H_2 production from alcoholic solutions. Moreover, the specific use of ethanol as a sacrificial agent could provide a good opportunity for the hydrogen photoproduction from a renewable source. This process has been largely studied over TiO_2-based systems but less research related with the use of ZnO-based photocatalysts has been performed. Most of the uses of nanostructured ZnO in photocatalysis have been related with the photodegradation of organics and dyes for environmental pollution control.

The band gap energy of ZnO (3.3 eV) is similar to that of TiO_2 and, ZnO shows a high exciton binding energy, 60 meV. Moreover, several efforts have been done to enhance the photocatalytic activity of ZnO by tailoring its morphology, particle size, and concentration of oxygen defects, surface facets and surface area. In this context, 1D-, 2D- and 3D-nanostructured ZnO has been prepared with different morphologies such as nanorods, nanowires, nanotubes, nanosheets and nanoflowers, among them, 1D nanostructures are considered good candidates as photocatalysts [1]. The delocalization of electrons in 1D nanostructures with high aspect ratios, favors the separation of photogenerated charge carriers improving the efficiency of photocatalysts.

In this work, we study the photocatalytic H_2 evolution from ethanol$_{(aq)}$ in gas phase at room temperature over pristine ZnO NWs. The characterization of the ZnO NWs, was carried out combining different techniques as FESEM, XRD, HRTEM), XPS, PL and Raman spectroscopy. The photocatalytic process was followed by *in-situ* diffuse reflectance infrared spectroscopy (DRIFTS) coupled to on-line mass spectrometry (MS) analysis. This allowed the determination of several surface species generated during the photocatalytic process, which are related with the products formed. The post-reaction ZnO NWs material was also analyzed.

2. Experimental

ZnO NWs were grown on a ZnO thin film, previously prepared from a polycrystalline zinc target of 99.99% purity and Ar/O_2 atmosphere over a Si(001) single crystal. For the *in-situ* photocatalytic DRIFTS-MS experiments, the samples were deposited into a reaction chamber and irradiated at λ=365 nm (20 mW·cm^{-2}) under a He flow saturated with ethanol/water vapor at room temperature. During irradiation, DRIFT and mass spectra were recorded as a function of time; the evolution of CH_3CH_2OH, CH_3CHO, CH_3COOH, CH_4, CO_2, CO and H_2 was continuously analyzed by MS.

3. Results and Discussion

3.1 Characteristics of photocatalysts

The morphology of the ZnO NWs was determined by FESEM. A uniform and dense array of ZnO NWs with average diameter of 50 nm, length of about 0.5 µm, and density between 40-80 NW.µm^{-2} was obtained. A specific surface area in the range of 15-30 m^2.g^{-1} was calculated using the FESEM average dimensions and assuming a cylindrical shape.

The XRD pattern of ZnO NWs (Fig. 1A) revealed the presence of mainly wurtzite ZnO (space group $P6_3mc$, JCPDS 00-036-1451), with cell parameters a≈3.25 Å and c≈5.20 Å, with very high [0001] preferred orientation and significant anisotropic peak enlargement. The 002 diffraction peak is splitted indicating that very probably there are two main different ZnO (0001) domains. According with XRD results, HRTEM analysis confirmed that ZnO NWs crystallize in the typical wurtzite structure and that ZnO NWs grow along the [0001] direction. Figure 1B shows a single ZnO NW visualized in the [-1100] direction. The Fourier transform image (inset in Fig. 1B) also accords with the only presence of several planes of wurtzite ZnO.

The XP spectrum corresponding to O 1s (Fig. 2a) is complex and can be deconvoluted into three components, the main component at 532 eV can be related with surface OH associated with surface defects and/or surface O^{2-} in oxygen-deficient regions [2]. The O 1s component centered at 530.1 eV is related with lattice O^{2-} and the very small component at 533.3 eV with chemisorbed oxygen-containing species [2]. The high intensity of the O 1s peak at 532 eV points to the presence of a large number of surface defects in the ZnO NWs.

Figure 3A shows the room-temperature PL emission spectrum of ZnO NWs, which show emissions in both the UV and visible spectral regions. The broad emission band observed in the visible range (430-830 nm) with maximum at around 650 nm (1.9 eV) can be attributed to the presence of different defects [3].

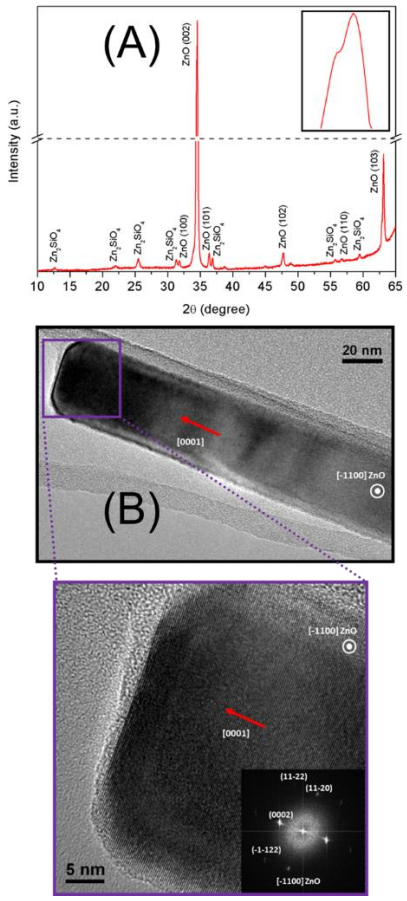

Fig. 1. A) XRD pattern of fresh ZnO NWs. In the inset, zoom of the ZnO (002) peak; B) TEM image of a ZnO NW visualized in the zone axis [-1100] and HRTEM micrograph of the marked zone; the inset shows the Fourier Transform image that corresponds to wurtzite ZnO.

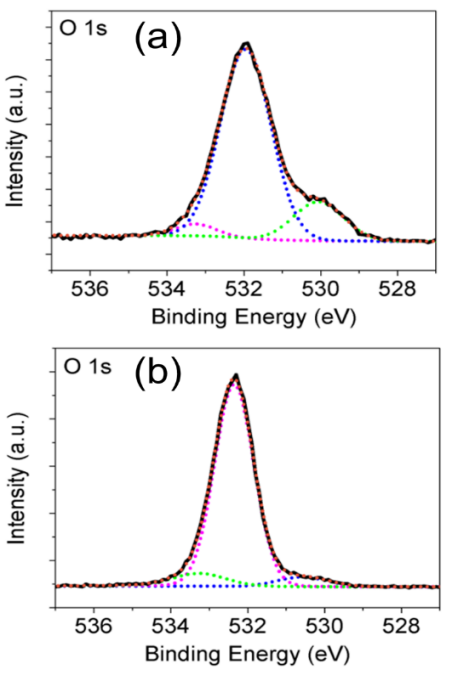

Fig. 2. O 1s core level spectra of ZnO NWs: a) fresh; b) post-reaction.

Finally, the Raman spectrum of the ZnO NWs (Fig. 3B) shows a wide band of low intensity at 400-500 cm^{-1} corresponding to the E_2 mode and a main well-defined band at about 580 cm^{-1}, which is related with the E_1(LO) mode and associated with oxygen deficiency [4].

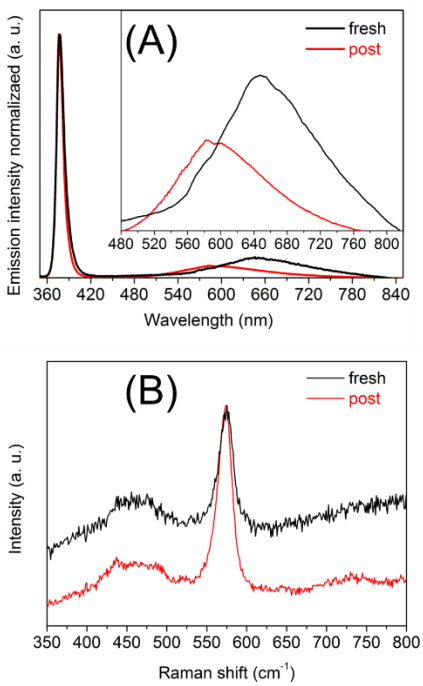

Fig. 3. A) Room-temperature PL spectra of fresh and post-reaction NWs; B) Raman spectra of fresh and post-reaction ZnO NWs.

3.2 Photocatalytic in-situ study

Figure 4A shows the analysis of the MS profiles of main products evolved during the *in-situ* irradiation process under continuous flowing of the ethanol/water vapor. Besides H_2, CO and CH_4, CO_2 and acetaldehyde were the main products; acetic acid and acetone were also detected. After switch off the irradiation, all products rapidly decreased in the outlet flow. The experiments carried out without illumination and the blank cell test, carried out without photocatalyst did not give any detectable product.

Figure 4B shows the DRIFT spectrum registered in the 1800-1300 cm^{-1} region during the *in-situ* irradiation process under continuous flowing of the ethanol/water vapor flow (spectrum a). The main band observed at 1742 cm^{-1} can be related with the presence of acetaldehyde (υ(C=O)).

Spectrum b in Figure 4B was obtained after the reaction quenching by switching off the light and stop the reactants flow. The bands centered at 1543 cm^{-1} and 1515 cm^{-1}, and 1385 cm^{-1} and about 1312 cm^{-1} can be related with the corresponding υ_{as}(COO) and υ_{s}(COO) modes of different acetate adsorbed species. Moreover, the contribution of different components to the very broad band centered at 1385 cm^{-1} can be proposed. Formate species over ZnO have been related with bands at 1385-1380 cm^{-1} (δ(CH)) and at about 1610 cm^{-1} (υ_{as}(COO)). Moreover, the υ_3 of free CO_3^{2-} ion is expected about 1440 cm^{-1}, and, other surface carbonate species could contribute to the broadness of the bands at 1543 cm^{-1} and 1515 cm^{-1}.

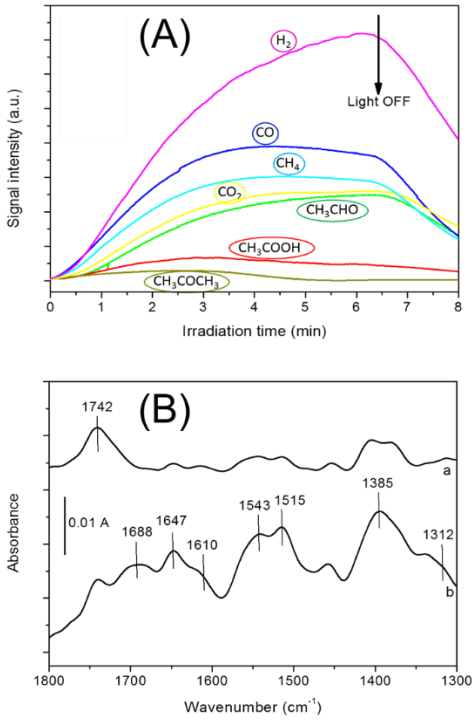

Fig. 4. A) Mass spectra profiles of different products evolved during the irradiation of ZnO NWs under a He flow saturated with ethanol/water vapor; B) *in-situ* DRIFT spectra of ZnO NWs: a) under irradiation and a He flow saturated with ethanol/water vapor; b) after (a), light off and switch the reactants flow to He flow.

On the other hand, a definite band centered at 1647 cm^{-1} has been related to the υ(C=O) of aldehyde species such as formaldehyde and/or unsaturated aldehydes. It is word of mention that in the quenching process (spectrum b in Fig. 4B), a band at 1688 cm^{-1} is clearly visible; this band can be attributed to the presence of surface acyl species, which could be the precursors of the surface carboxylate species detected. On the basis of these results and previous studies on photoreforming of ethanol [5], we propose several processes that could take place over ZnO NWs during the irradiation of an ethanol/water flow at room temperature. The first step could be the photocatalytic transformation of ethanol into acetaldehyde and H_2. Once acetaldehyde is formed, the photocatalytic reaction of $acetaldehyde_{(aq)}$ could produce acetic acid and H_2; acetaldehyde could also decompose forming CO and CH_4. CO_2 could come from the acid acetic photodecomposition or from the $acid\ acetic_{(aq)}$ photoreforming.

In order to compare the evolution under irradiation of the surface species formed after ethanol/water adsorption, separate *in-situ* DRIFTS-MS experiments were carried out over ZnO NWs and a reference ZnO thin film material. The results indicate that the surface species generated after adsorption of ethanol/water over ZnO NWs, are easily phototransformed at room temperature, and contrarily, irreversible carboxylate (and/or carbonate) species remains under irradiation on the reference ZnO film material.

After the *in-situ* DRIFTS-MS photocatalytic reaction, the ZnO NWs were analyzed by FESEM, XRD, XPS, PL and Raman spectroscopy. No significant changes in the ZnO NWs were observed in morphology, structure and surface characteristics. On the other hand, Figure 3A and 3B show the PL emission and Raman spectra, respectively, of the post-reaction ZnO NWs. Slight differences in the position and broadness of the visible emission band (Fig. 3A) can be observed. It has been proposed that defects are related with the shift observed, due to a slight modification of the energy band structure of ZnO; the broadening observed on the FWHM indicates that the quantity of intrinsic defects is higher for the fresh sample [3]. In the same line, some differences can be also observed in the Raman E_1(LO) mode when comparing the phonon frequencies and the FWHM of the peak at around 580 cm^{-1} for the fresh and the post-reaction samples (Fig. 4B). The used photocatalyst reaction exhibits a small blue shift (1.4 cm^{-1}) and a decrease of the mode line width (FWHM by 1 cm^{-1}) when compared to the fresh sample; existence of defects would result in a broadening of the peak at around 580 cm^{-1} [4].

4. Conclusions

ZnO nanowires with wurzite structure and a very high [0001] preferred orientation were active in the photocatalytic hydrogen production from ethanol(aq) in gas phase. The photocatalytic behavior has been related with the 1D nanostructure characteristics of ZnO NWs. The combination of different techniques allowed us to identify the presence of different defects in the ZnO NWs such as oxygen vacancies, which are related with their catalytic performance. After the *in-situ* DRIFTS-MS photocatalytic study carried out, we propose several processes that could take place. First step could be the formation of acetaldehyde and H_2. Then, photocatalytic transformation of acetaldehyde in the presence of water vapor could produce acetic acid and H_2. However, acetaldehyde also decomposes forming CO and CH_4. The acid acetic photo-decomposition or photo-reforming results in the CO_2 formation. The characteristics of ZnO NWs resulted almost unaltered after the photocatalytic process.

Acknowledgements

The authors aknowledge the financial support of projects MAT2017-87500-P and PID2020-116031RBI00/AEI/10.13039/501100011033/FEDER and IREC and CCiTUB facilities.

References

[1] F. Ahmed, N. Arshi, M.S. Anwar, R. Danish, B.H. Koo, RSC Advances 4 (2014) 29249-29263.
[2] X. Zhang, J. Qin, Y. Xue, P. Yu, B. Zhang, L. Wang, R. Liu, Sci. Rep. 4 (2014) 4596.
[3] Y. Feng, G. Wang, J. Liao, W. Li, C. Chen, M. Li, Z. Li, Sci Rep. 7 (2017) 11622.
[4] F. Güell, P. R. Martínez-Alanis, S. Khachadorian, J. Rubio-Garcia, A. Franke, A. Hoffmann, G. Santana, Phys. Stat. Sol. B 253 (2016) 883-888.
[5] A.C. Sola, N. Homs, P. Ramírez de la Piscina, Int. J. Hydrogen Energy, 41 (2016).